npg

Open

ORIGINAL ARTICLE

Intragenic DNA methylation modulates alternative splicing by recruiting MeCP2 to promote exon recognition

Alika K Maunakea[1, 2, *], Iouri Chepelev[1, 3, *], Kairong Cui[1], Keji Zhao[1]

[1]*Systems Biology Center, National Heart, Lung and Blood Institute, NIH, Bethesda, MD 20892, USA*

Although the function of DNA methylation in gene promoter regions is well established in transcriptional repression, the function of the evolutionarily conserved widespread distribution of DNA methylation in gene body regions remains incompletely understood. Here, we show that DNA methylation is enriched in included alternatively spliced exons (ASEs), and that inhibition of DNA methylation results in aberrant splicing of ASEs. The methyl-CpG-binding protein MeCP2 is enriched in included ASEs, particularly those that are also highly methylated, and inhibition of DNA methylation disrupts specific targeting of MeCP2 to exons. Interestingly, ablation of MeCP2 results in increased histone acetylation and aberrant ASE-skipping events. We further show that inhibition of histone deacetylase (HDAC) activity leads to exon skipping that shows a highly significant degree of overlap with that caused by *MeCP2* knockdown. Together, our data indicate that intragenic DNA methylation operates in exon definition to modulate alternative RNA splicing and can enhance exon recognition via recruitment of the multifunctional protein MeCP2, which thereby maintains local histone hypoacetylation through the subsequent recruitment of HDACs.

Introduction

In mammals, DNA methylation is essential for embryonic development, differentiation, cell cycle control, and maintenance of genome stability [1, 2]. At promoters, DNA methylation generally precludes transcription directly by blocking the binding of transcriptional activators or indirectly through the recruitment of methyl-binding proteins and co-repressor complexes containing histone deacetylases (HDACs), which cooperatively facilitate the formation of heterochromatin [3]. However, recent genome-wide studies have revealed that DNA methylation occurs far more frequently within gene bodies than at promoters [4-7]. Preferential positioning of DNA methylation over exons compared with introns [8-11] prompted speculation for its potential role in pre-mRNA splicing regulation, which however remains largely unsubstantiated. Indeed, a recent study showed that DNA methylation and CTCF binding play mutually exclusive roles in affecting pre-mRNA splicing by inhibiting and promoting the recognition of an alternatively spliced exon, respectively [12]. The kinetic model for the coupling of transcriptional elongation with alternative splicing [13] and the demonstration that intragenic DNA methylation affects elongation efficiency [14] make it likely that DNA methylation at exons would reduce transcriptional elongation rate and promote exon inclusion. However, the extent to which DNA methylation functions in splicing regulation and whether it plays a positive role in exon inclusion are currently not known.

In this study, we sought to determine whether the intragenic DNA methylation is involved in pre-mRNA splicing regulation and if so, whether it involves the methyl-CpG-binding protein, MeCP2. Here, we show that DNA methylation is significantly enriched in included alternatively spliced exons (ASEs) as compared with excluded ASEs. Chemical or genetic perturbation

of DNA methylation led to aberrant splicing of ASEs. Combined analyses of our results from the ChIP-Seq and RNA interference experiments revealed that MeCP2 contextualizes exon methylation by functioning primarily in promoting recognition of ASEs for inclusion. Our data also suggest that DNA methylation affects ASE splicing by recruiting MeCP2 and subsequent HDAC activities.

Results

CpG methylation level is elevated in included ASEs as compared with excluded ASEs

Recent genome-wide analyses of CpG methylation reveal a preferential positioning of DNA methylation over exons compared with introns [8-11], suggesting a potential role of DNA methylation in pre-mRNA splicing regulation. To test whether there is a functional link between DNA methylation and splicing, we decided to ex-

amine how DNA methylation is related to ASE splicing. Using paired-end RNA-Seq, we first determined gene expression levels and splicing patterns genome-wide in two human cell lines. As shown in the cartoon in Figure 1A, inclusion of the ASE in the final spliced mRNA product generates transcript N1 and exclusion of the ASE generates transcript N2. If N1 occupies $\geq$ 90% of the sum of N1 + N2, then the ASE is defined as included; if N1 occupies $\leq$ 10% of the sum of N1 + N2, then the ASE is defined as excluded. Using this criterion, we identified 6 534 included ASEs and 3 604 excluded ASEs in IMR90 cells (Figure 1A). Similarly, we identified 4 925 and 3 867 included and excluded exons, respectively, in HCT116 cells (Figure 1A).

Using published single-base resolution DNA methylome data in IMR90 cells [15], we examined the CpG methylation levels at the ASEs and their 5′ and 3′ neighboring exons. This analysis revealed that included ASEs
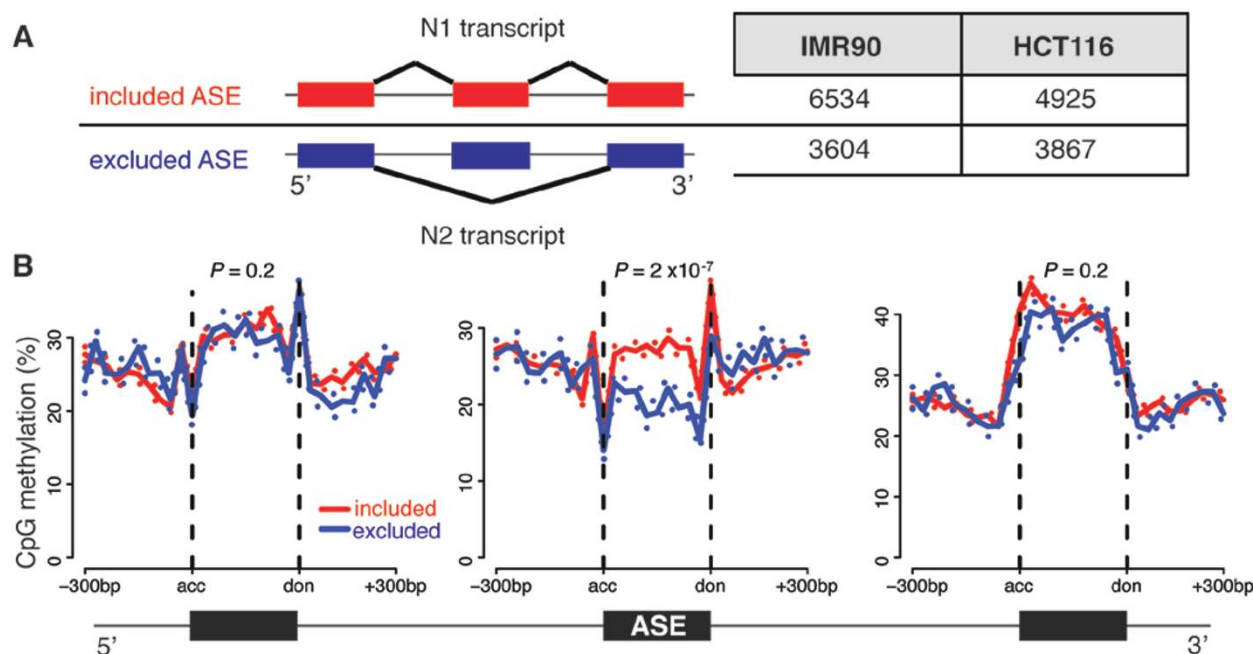

Figure 1 DNA methylation is enriched in included ASEs. **(A)** The cartoon on the left indicates the cassette exons: an ASE flanked by two constitutively spliced exons. "N1 transcript" represents the spliced RNA product that includes the ASE (red) and "N2 transcript" represents the spliced RNA product that excludes the ASE (blue). To detect the alternative splicing events, RNA was isolated from IMR90 or HCT116 cells and profiled using RNA-Seq. Numbers of included and excluded annotated ASEs of expressed genes, which were identified using MISO from the RNA-Seq data, are listed in the table. **(B)** DNA methylation level is significantly higher over included ASEs than excluded ASEs. CpG methylation levels were calculated from published data of IMR90 cells [15], within cassette exons from the two ASE groups described in **A** and the methylation levels were displayed in ± 300-bp windows relative to the splice acceptor (acc) and donor (don) sites across the cassette exons. The higher level of CpG methylation in included than excluded ASEs observed from this analysis is consistent with the higher level of CpG methylation in included exons demonstrated in an earlier report [10]. A schematic representation of the ASE and flanking exons is displayed, oriented to the direction of transcription. The *P*-values for the relative enrichment of CpG methylation in included compared to excluded exons were calculated using one-sided *t*-test for the normalized DNA methylation level in the exons.

were associated with significantly higher levels of DNA methylation than excluded ASEs (Figure 1B). This pattern is specific to ASEs as their surrounding constitutive exons did not exhibit significant differences in DNA methylation. These results indicate that DNA methylation may be involved in the regulation of ASE inclusion.

DNA methylation is involved in the regulation of RNA splicing

To directly test whether inhibition of DNA methylation results in defects in pre-mRNA splicing, we treated IMR90 cells with 5′-aza-2′-deoxycytidine (5azadC), which is known to reduce global levels of DNA methylation, albeit inefficiently [16]. To overcome this potential limitation, we took advantage of engineered HCT116 cells that express hypomorphic *DNMT1* and lack *DNMT3b* (HCT116-DKO), resulting in genome-wide loss of CpG methylation [17]. We confirmed the effects of DNA demethylation in these two cell systems by demonstrating that the expression of several known imprinted genes was induced by global demethylation (Supplementary information, Figure S1). Using the paired-end RNA-Seq assays, we compared the expression of the annotated ASE junctions between control and demethylated cells. Our analyses revealed that 5azadC treatment resulted in significant downregulation (increased exclusion) of 753 ASEs and upregulation (increased inclusion) of 877 ASEs in IMR90 cells (Figure 2A). Similarly, DNMT-deficiency caused downregulation of 641 ASEs and upregulation of 730 ASEs in HCT116 cells (Figure 2A). We found that the extent of ASE downregulation following 5azadC treatment in IMR90 cells was dependent on the original DNA methylation level of the ASE (Figure 2B). This observation suggests that although demethylation resulted in nearly equivalent numbers of increased ASE exclusion and inclusion events, ASEs with high levels (> 70%) of DNA methylation are more likely to be downregulated than ASEs with low levels (< 30%) of DNA methylation, indicating that DNA methylation may function in exon inclusion. Although exon exclusion and inclusion events appear to be affected by global changes of DNA methylation, we cannot decisively conclude that changes in DNA methylation directly alter splicing of exons. For example, 5azadC treatment has been shown to inhibit histone methylation [18], intragenic levels of which could influence splicing [19].

Next, in order to directly confirm the changes of DNA methylation in affected exons, we examined the DNA methylation level at exon 10 of the *HAUS8* gene, which was aberrantly skipped as a result of demethylation (Figure 2C). Exon 10 of *HAUS8* harbors methylated CpGs in HCT116 and IMR90 cells (Figure 2C). Although this exon is normally included in control cells (HCT116-WT and IMR90-CTR), we detected exon junctions that skip this exon in both HCT116-DKO and 5azadC-treated IMR90 cells (highlighted in red in Figure 2C). Using bisulfite PCR-sequencing assays, we observed significantly decreased DNA methylation levels at the exon 10 in HCT116-DKO cells compared with HCT116-WT cells (Figure 2D). Together, these results indicate that DNA methylation may be directly involved in facilitating exon inclusion.

MeCP2 binding is enriched in exons and is dependent on CpG methylation

Although it has been reported that DNA methylation inhibits CTCF binding to *CD45* exon 5, leading to exon 5 exclusion [12], it is still possible that DNA methylation may facilitate exon inclusion in other settings by recruiting methyl-binding domain (MBD) proteins. Based on the known ability of MeCP2 to recognize single methyl-CpGs *in vitro* [20] and previous evidence implicating its role in splicing regulation [21, 22], we focused our investigation on MeCP2 and determined its genome-wide binding profile in IMR90 cells using ChIP-Seq. The antibody used for ChIP-Seq was specific to MeCP2 as determined by western blot assays and enriched a sequence within the imprinted gene *SNRPN* known to be bound by MeCP2 *in vivo* [23] (Supplementary information, Figure S2). Consistent with its role in regulating transcription [24], MeCP2 preferentially occupies promoters (Figure 3A). Interestingly, we found that MeCP2 is also enriched in exonic regions (Figure 3A), consistent with its potential role in splicing regulation.

Next, we tested whether MeCP2 binding tracks with intragenic DNA methylation by integrating the high-resolution genome-wide bisulfite-sequencing data of CpG methylation in IMR90 cells [15] with our data of the genome-wide MeCP2 distribution. To test whether MeCP2 binding is correlated with DNA methylation at the exons, we divided all the exons into two groups based on their DNA methylation levels (Figure 3B). This analysis revealed that exons with higher levels (50% - 100%) of DNA methylation also harbor significantly higher levels of MeCP2 than exons with lower levels (0% - 50%) of DNA methylation (Figure 3B). To quantitatively substantiate that MeCP2 binding tracks with DNA methylation at exons, we devised a sensitive rank-based test to determine the overlap between MeCP2 binding and DNA methylation. The observed overlap between MeCP2 occupancy and DNA methylation at exons arose significantly more often than expected by chance (Figure 3C). Taken together, these data indicate that MeCP2 binding is linked to DNA methylation of exons.
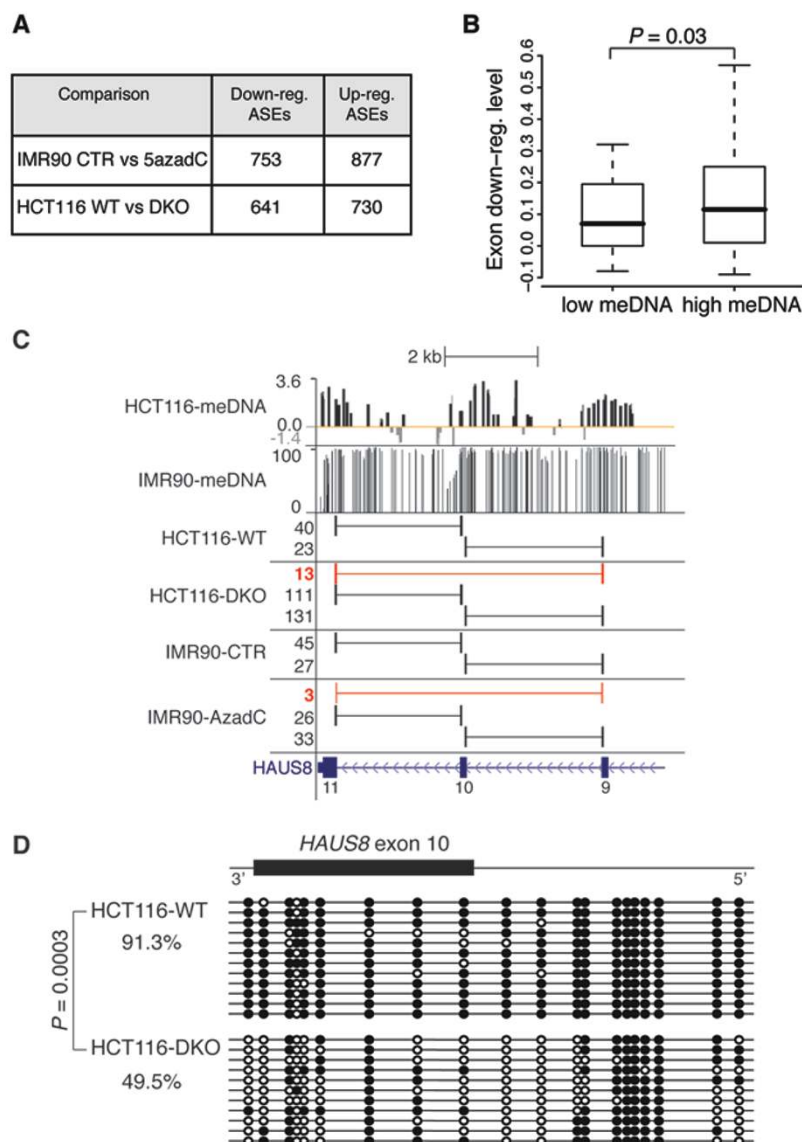
Figure 2 DNA methylation functions in pre-mRNA splicing. **(A)** DNA methylation is involved in splicing. To detect the function of DNA methylation in splicing, RNAs isolated from 5azadC-treated and control (CTR) IMR90 cells were profiled using RNA-Seq. Similarly, RNAs isolated from HCT116-WT or HCT116-DKO cells were profiled using RNA-Seq. The significantly changed exons were identified using MISO from the RNA-Seq data. The table lists the numbers of the significantly downregulated and upregulated exons induced by DNA methylation inhibition. **(B)** Hypermethylated exons have a higher tendency to be downregulated than hypomethylated exons following inhibition of DNA methylation by 5azadC treatment in IMR90 cells. The degree of exon downregulation was calculated and compared between hypermethylated and hypomethylated included exons. High meDNA indicates ASE with > 70% CpG methylation and low meDNA indicates ASE with < 30% CpG methylation. *P*-value was calculated by one-sided KS test. **(C)** Inhibition of DNA methylation leads to skipping of exon 10 of the *HAUS8* gene in the spliced product. UCSC browser display of indicated data (NCBI36/hg18 assembly) over coordinates chr19:17,021,565-17,029,029 for *HAUS8* focusing on the last three RefSeq annotated exons. DNA methylation data from HCT116-WT and IMR90 cells were obtained from public sources and displayed accordingly [15, 46]. Exon junctions from paired-end RNA-Seq data from 5azadC-treated IMR90 cells and HCT116-DKO cells and their respective control cells are displayed, where red indicates aberrant skipping events and black indicates normal "full-length" transcript. The number of tags representing each exon junction is shown to the left of the junctions. Exons are labeled according to RefSeq. meDNA: DNA methylation. **(D)** Comparison of DNA methylation in unperturbed (HCT116-WT) and demethylated (HCT116-DKO) cells in the *HAUS8* exon 10 region. DNA methylation was determined by the bisulfite-sequencing of the *HAUS8* exon 10 region. Each colored circle represents individual CpG cytosine methylation status within the analyzed region (black: methylated; white: unmethylated). Percentage of methylation was determined based on the number of methylated CpG cytosines divided by the total number of CpG cytosines within the analyzed sequences from all the PCR clones. *P*-value shown was calculated using one-sided Student's *t*-test.
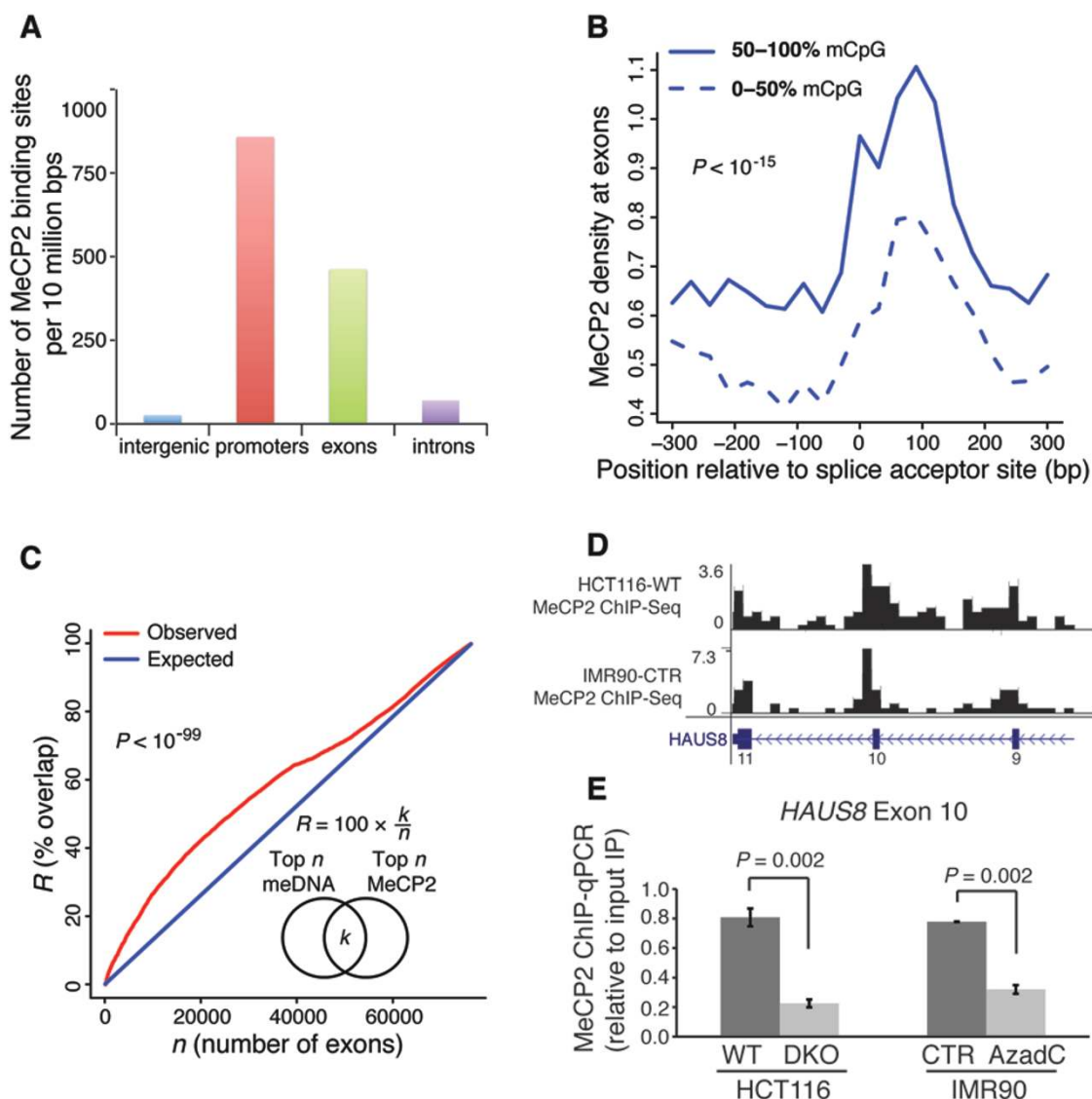
Figure 3 MeCP2 exhibits DNA methylation-dependent binding to exons. **(A)** MeCP2 is enriched in promoters and exonic regions. MeCP2-binding profile in IMR90 cells was determined using ChIP-Seq and its distribution is displayed by normalizing to the genomic size of each indicated category. **(B)** High MeCP2 density correlates with high levels of DNA methylation in IMR90 cells. The MeCP2 densities at exons sorted according to DNA methylation levels as indicated are displayed. *P*-value was calculated by one-sided KS test. **(C)** Co-localization of MeCP2 and methylated DNA within exons occurs significantly more often than expected by random chance. The set of top *n* MeCP2-enriched exons shares *k* exons with the set of top *n* DNA-methylated exons. For each value *n* (*x*-axis), the overlap percentage *R* (*y*-axis) of the two sets is shown by a red curve. The overlap percentage expected by random chance is shown as a blue curve. **(D)** UCSC Genome Browser tracks showing MeCP2 ChIP-Seq data in HCT116 and IMR90 cells. The region shown contains exons 9-11 of the *HAUS8* gene. **(E)** MeCP2 binding at the aberrantly skipped exon 10 of *HAUS8* is significantly reduced upon DNA demethylation. MeCP2 binding was measured relative to input chromatin in the indicated cells by ChIP-qPCR. Error bars represent SE. *P*-values shown were calculated using one-sided Student's *t*-test.

To test whether DNA methylation facilitates MeCP2 binding to exonic regions, we examined the changes in local MeCP2 occupancy caused by inhibition of DNA methylation using qPCR assays over the exons that were aberrantly skipped upon global DNA demethylation. We found that MeCP2 binding was highly enriched at exon 10 of *HAUS8* in HCT116 cells and IMR90 cells (Figure 3D), and that genetic or chemical inhibition of DNA methylation substantially decreased MeCP2 binding in these two cell lines (Figure 3E). These results suggest
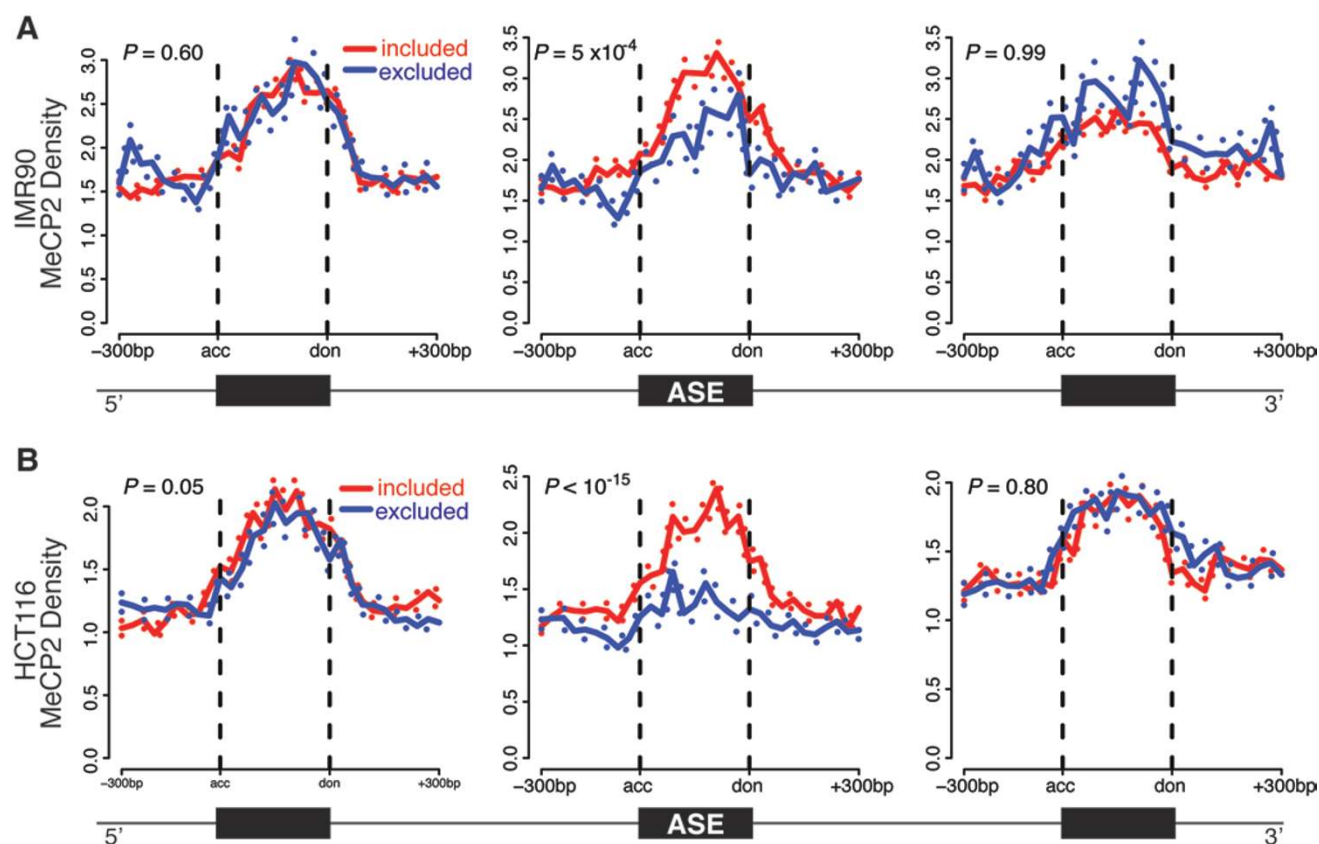
Figure 4 MeCP2 is significantly enriched in included ASEs. **(A)** MeCP2 density is higher in included compared with excluded ASEs in IMR90 cells. The MeCP2 densities at the included and excluded ASEs and their flanking constitutively spliced exons in IMR90 cells were measured by ChIP-Seq and displayed in ± 300-bp surrounding the displayed exon. Schematic of the ASE and the flanking exons is displayed below each graph. **(B)** MeCP2 density is higher in included compared with excluded ASEs in HCT116 cells. Data are displayed as in **A**. All *P*-values displayed in **A** and **B** were calculated by one-sided KS test.

that CpG methylation recruits MeCP2 to exons.

MeCP2 binding is significantly enriched in included ASEs and positively regulates ASE inclusion

To further examine whether MeCP2 binding is correlated with exon inclusion in a particular cell type, we plotted the profiles of MeCP2 binding at the annotated ASEs that were identified in IMR90 and HCT116 cells. This analysis revealed that the included ASEs were associated with significantly higher levels of MeCP2 binding than excluded ASEs (Figure 4). This pattern is concordant in both cell types examined and, importantly, is specific to ASEs as their surrounding constitutive exons did not exhibit significant differences in MeCP2 density (Figure 4). These results indicate that MeCP2 may be involved in the DNA methylation-dependent ASE inclusion events, and that it might function to enhance the inclusion of the ASEs.

To directly test the function of MeCP2 in splicing, we

depleted *MeCP2* expression using shRNAs in IMR90 and HCT116 cells (Figure 5A and 5B) and examined the numbers of ASE inclusion and exclusion events in these cells (Figure 5C). Indeed, upon *MeCP2* knockdown, 1 800 exons were aberrantly excluded, while only 664 exons were aberrantly included in IMR90 cells (Figure 5C). Similarly, *MeCP2* knockdown in HCT116 cells generated more aberrantly excluded exons (2 856) than included exons (1 918) (Figure 5C). These results support the notion that MeCP2 promotes exon recognition and inclusion.

To determine whether these altered splicing events are directly correlated with MeCP2 binding, we compared the levels of local MeCP2 density in untreated IMR90 cells between ASEs that become aberrantly excluded and aberrantly included upon *MeCP2* knockdown. ASEs that become aberrantly excluded upon *MeCP2* knockdown originally harbor significantly higher levels of MeCP2 density than ASEs that become aberrantly included (Fig-
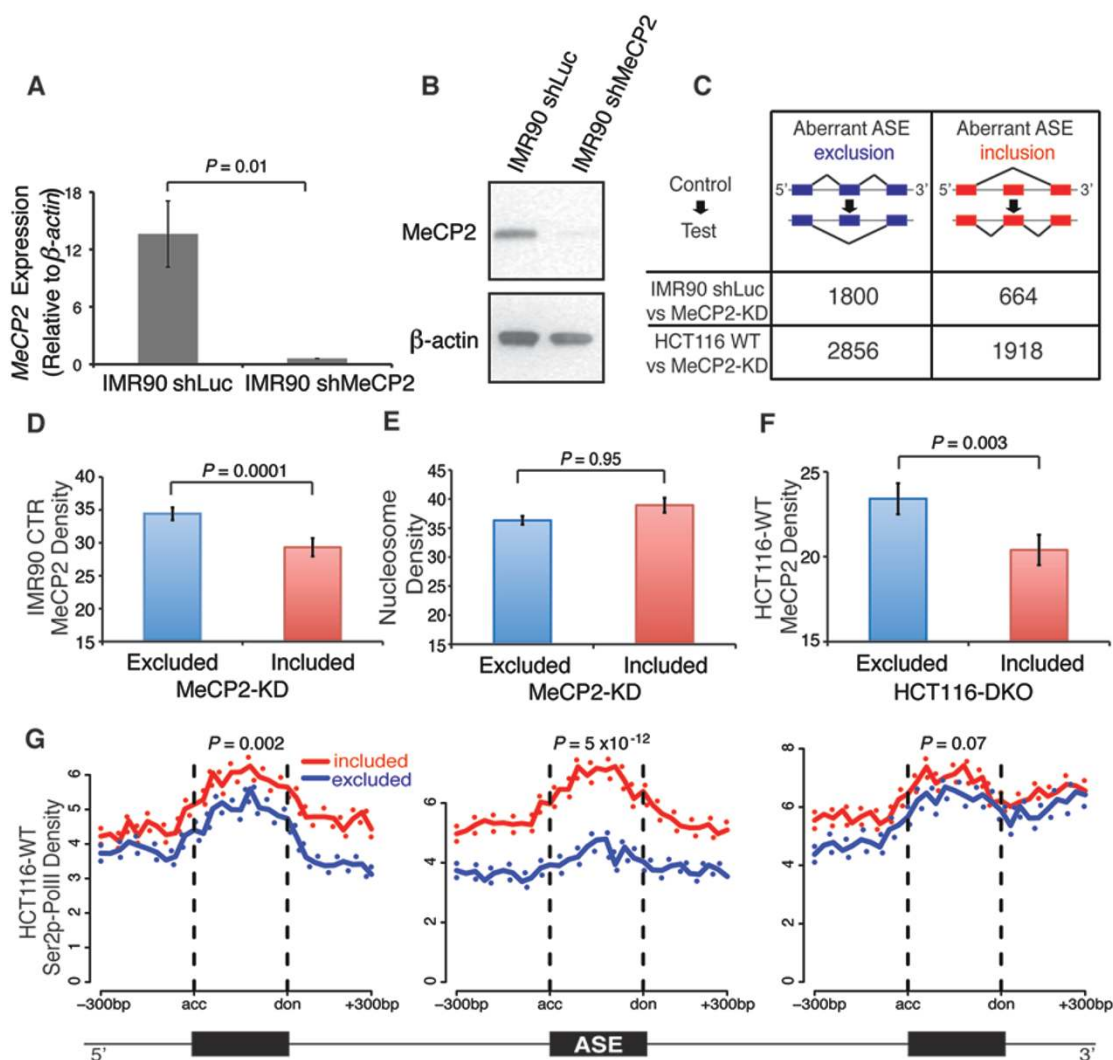
Figure 5 MeCP2 is critically involved in ASE inclusion in the spliced RNA products. **(A)** Significantly reduced *MeCP2* mRNA levels in IMR90 cells upon *MeCP2* knockdown. *MeCP2* expression in IMR90 cells infected with viruses containing the negative control shRNA-luciferase (shLuc) construct or shRNA-MeCP2 (shMeCP2) construct was measured in triplicate using real-time qPCR and calculated as a percentage relative to *β-actin* mRNA levels using the delta-C_t method. Error bars represent SE. *P*-value shown was calculated using one-sided Student's *t*-test. **(B)** Reduced MeCP2 protein levels in IMR90 cells infected with viruses containing a shRNA-MeCP2 construct. MeCP2 protein expression in IMR90-shLuc and IMR90-shMeCP2 cells was measured by the western blot assays using the same antibody for ChIP-Seq experiments. β-Actin serves an internal control. **(C)** Knockdown of *MeCP2* results in aberrant alternative splicing events. Schematic representation of aberrant exon downregulation and upregulation upon *MeCP2* knockdown is displayed above the table listing the total numbers of these events in IMR 90 and HCT116 cells. For both cell lines, shLuc serves as a control shRNA construct, MeCP2-KD represents *MeCP2* knockdown mediated by a specific shRNA. Higher number of aberrant ASE downregulation than upregulation events occur upon *MeCP2* knockdown for both IMR90 and HCT116 ($P < 10^{-100}$, one-sided binomial test). **(D)** The original MeCP2 density is higher in the ASEs that become aberrantly downregulated than those that become upregulated upon *MeCP2* knockdown. MeCP2 densities of the ASEs were measured in shLuc-transduced IMR90 cells by ChIP-Seq. **(E)** Nucleosome density is not significantly different between exons that become aberrantly upregulated and those that become downregulated upon *MeCP2* knockdown. The average nucleosome densities for each ASE group were calculated based on data from IMR90 cells from the GEO database (GSE21823). **(F)** The original MeCP2 density in HCT116-WT cells is higher in ASEs that become aberrantly downregulated than those that become upregulated in HCT116-DKO cells. Average MeCP2 densities were calculated for each indicated group from ChIP-Seq data of HCT116-WT cells. *P*-values displayed in **D**-**F** were calculated by one-sided Wilcoxon test. **(G)** Ser2P-Pol II is significantly enriched in included ASEs. Ser2P-Pol II density is higher in included than excluded ASEs in HCT116 cells. The Ser2P-Pol II densities at included and excluded ASEs and their flanking constitutively spliced exons in HCT116 cells were measured by ChIP-Seq and displayed in ± 300 bp surrounding the displayed exon. Schematic of the ASE and flanking exons is displayed below each graph. All *P*-values displayed were calculated by one-sided Student's *t*-test.

ure 5D), supporting that loss of local MeCP2 binding results in exon skipping. As a negative control, we did not observe a similar trend for nucleosome density between these two groups of ASEs in untreated IMR90 cells (Figure 5E), suggesting that the positive role of MeCP2 in regulating exon inclusion is specific. We also observed that the local MeCP2 density in HCT116-WT cells was significantly higher in ASEs that become aberrantly excluded in HCT116-DKO cells (Figure 5F). Altogether, these findings provide evidence that DNA methylation-dependent MeCP2 binding enhances ASE inclusion.

Established mechanisms for alternative splicing regulation involve transcriptional elongation [13, 25]. To determine whether MeCP2 binding regulates ASE inclusion via modulating transcriptional elongation, we performed ChIP-Seq analysis of transcriptionally engaged and elongating RNA polymerase II (Ser2P) in HCT116-WT cells. Similar to the MeCP2-binding profiles (Figure 4), Ser2P-Pol II levels were significantly higher precisely at included ASEs than excluded ASEs (Figure 5G). Interestingly, Ser2P-Pol II is depleted over the excluded ASEs (blue line, middle graph), whereas it is enriched over the constitutively spliced exons flanking either included or excluded ASEs (left and right graphs) and over included ASEs (red line, middle graph) relative to their respective surrounding intronic regions (Figure 5G). This pattern of Ser2P-Pol II depletion specific to excluded ASEs is highly significant relative to Ser2P-Pol II enrichment in included ASEs and the flanking constitutive exons ($P = 2 \times 10^{-9}$, the *P*-value was calculated by Student's *t*-test as described in Materials and Methods). Together, these results suggest a mechanism for the involvement of MeCP2 in splicing regulation, which is likely coupled to the kinetics of Pol II-mediated transcriptional elongation.

HDACs mediate the activity of MeCP2 in ASE inclusion

As MeCP2 is known to recruit HDACs to target genes for transcriptional repression [24], we tested whether MeCP2 modulates splicing of ASEs via recruiting the activities of HDACs. Thus, we inhibited HDAC activities by treating cells with trichostatin-A (TSA), and then analyzed splicing events using RNA-Seq. Interestingly, treatment of HCT116 cells with TSA for 6 h resulted in significantly more aberrant downregulation of ASEs (3 693) than upregulation of ASEs (2 280) (Figure 6A). Similarly, significantly more aberrant downregulation (2 736 ASEs) than aberrant upregulation events (1 454 ASEs) were detected after the TSA treatment in IMR90 cells (Figure 6A). These results indicate that HDACs are involved in the regulation of alternative splicing, and primarily enhance ASE inclusion in these cells, which is similar to the function of MeCP2 (Figure 5C). To test

whether MeCP2 and HDACs regulate ASE inclusion through a shared pathway, we analyzed the extent to which their target ASEs overlap. Indeed, highly significant overlaps were detected: 32% and 20% in IMR90 and HCT116 cells, respectively (Figure 6B and 6C). Interestingly, we found a significantly higher degree of overlap in the downregulated ASEs than the upregulated ASEs in both HCT116 cells (20% down vs 11% up) and IMR90 cells (32% down vs 12% up) (Figure 6D). These results support our hypothesis that MeCP2 and HDACs function to enhance ASE inclusion through a shared pathway.

MeCP2 binding to ASEs is dependent on CpG methylation but not histone acetylation

If MeCP2 functions to facilitate ASE inclusion via recruiting HDAC activity, knockdown of *MeCP2* may lead to increased histone acetylation at the affected ASEs. To test this, we performed ChIP-qPCR assays to analyze MeCP2 binding and histone acetylation at the *FAM204A* gene locus. The second exon of *FAM204A* is the only known ASE of the gene (Figure 7A). In HCT116-WT cells, this ASE was included in 60% of the *FAM204A* transcripts (Figure 7B). In HCT116-DKO cells, the ASE inclusion was reduced to 37%. Similarly, both TSA-treated and *MeCP2*-knockdown cells exhibited significantly decreased levels of ASE inclusion compared with wild-type cells (Figure 7B). Using ChIP-qPCR assays, we detected significantly decreased binding of MeCP2 at both the ASE and its 5′ adjacent exon of *FAM204A* upon *MeCP2* knockdown (Figure 7C). Concomitantly, we observed substantial increases in histone H4 acetylation levels over the ASE but not over the constitutively spliced neighboring exons upon *MeCP2* knockdown (Figure 7D), indicating that MeCP2 recruits HDACs to modulate histone acetylation at the ASE. These findings are consistent with previous studies showing the potential involvement of histone acetylation in alternative splicing regulation [19, 26, 27].

To further test the temporal relationship of CpG methylation, MeCP2 binding, and histone deacetylation, we analyzed MeCP2 binding and histone acetylation levels at the *FAM204A* ASE in HCT116-WT and HCT116-DKO cells. These data showed that DNA hypomethylation resulted in significantly decreased binding of MeCP2 to the ASE (Figure 7E) and substantially increased local histone H4 acetylation levels (Figure 7F), indicating that DNA methylation acts upstream of MeCP2 binding and HDAC-mediated deacetylation. In further clarifying the order of MeCP2 binding and HDAC-mediated deacetylation, we found that TSA treatment did not affect the binding of MeCP2 to the ASE (Figure 7G). Therefore, these data, together with the finding that *MeCP2* knock-
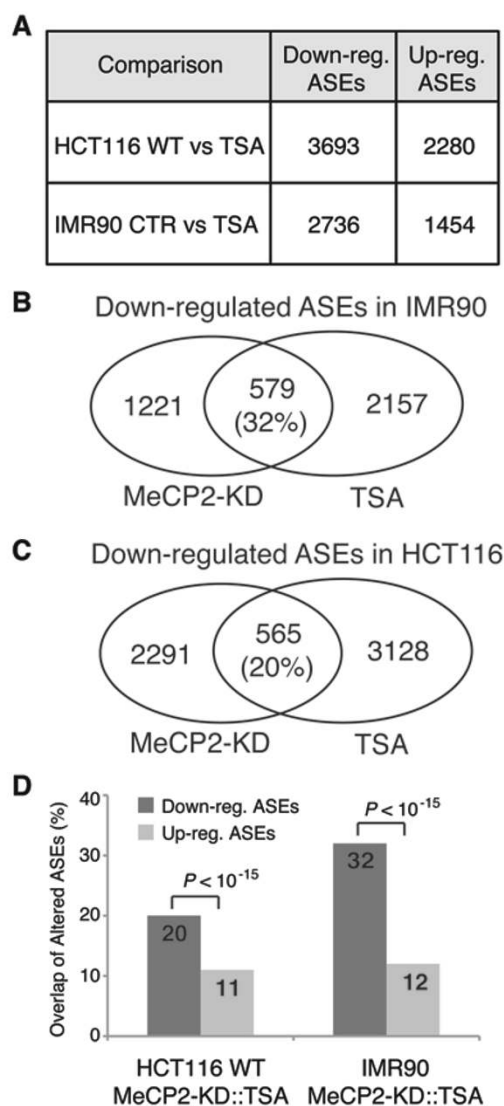
Figure 6 Inhibition of HDACs results in aberrant ASE exclusion events that significantly overlap with those caused by MeCP2 knockdown. **(A)** Genome-wide alteration of splicing events is induced by TSA treatment. The total numbers of significantly downregulated (Down-reg.; aberrantly excluded) and upregulated (Up-reg.; aberrantly included) ASEs in TSA-treated HCT116-WT cells and TSA-treated IMR90 cells in comparison to their respective untreated control cells are displayed. There is significantly higher numbers of downregulated ASEs than upregulated ASEs in both cell types ($P < 10^{-100}$, one-sided binomial test). **(B)** Venn diagram showing the overlap between the aberrantly excluded ASEs upon MeCP2 knockdown and aberrantly excluded ASEs induced by TSA treatment in IMR90 cells. **(C)** Venn diagram showing the overlap between the aberrantly excluded ASEs upon MeCP2 knockdown and aberrantly excluded ASEs induced by TSA treatment in HCT116 cells. **(D)** Downregulated rather than upregulated ASEs induced by either *MeCP2*-knockdown or TSA treatment frequently occur together. RNA-Seq data of altered ASE expression from control and MeCP2-KD or TSA-treated HCT116 and IMR90 cells were compared. *P*-values were calculated using χ^2-test.

down led to increases in histone acetylation levels at the ASE (Figure 7D), suggest that MeCP2 binding operates upstream of histone deacetylation by recruiting HDAC activities to the ASE.

Discussion

Although incompletely understood, intragenic DNA methylation exerts multiple potential functions such as reducing gene expression by regulating transcriptional elongation efficiency [14], determining alternative polyA site choice [28] and tissue-specific selection of alternative promoters [7]. Our study substantiates an additional function for intragenic DNA methylation and provides a novel mechanism for the positive regulation of ASE inclusion in pre-mRNA splicing. As summarized in Figure 7H, we found that (1) chemical or genetic inhibition of DNA methylation that is highly enriched in included ASEs resulted in extensive splicing defects such as aberrant exon exclusion; (2) knocking down *MeCP2*, which is significantly enriched in included ASEs depending on DNA methylation levels, primarily led to aberrant ASE exclusion events in both HCT116 and IMR90 cells; and (3) chemical inhibition of HDAC activity also primarily led to aberrant ASE exclusion events that significantly overlap with those induced by *MeCP2* knockdown. Furthermore, inhibition of DNA methylation or MeCP2 expression caused increased acetylation levels over aberrantly excluded ASEs. Based on these results, we propose that exonic DNA methylation acts to recruit or enhance MeCP2 binding, which subsequently facilitates recruitment of HDACs to maintain a low acetylation level of the underlying ASE for its efficient inclusion in the spliced mRNA transcripts (Figure 7I).

Plausible mechanisms for the enhanced ASE inclusion by histone deacetylation include: (a) histone hypoacetylation at specific ASEs caused by HDACs influences the rate of local Pol II elongation and subsequently the efficiency of ASE inclusion [27], (b) the binding of MeCP2-containing complexes to DNA methylation-enriched exons reduces the efficiency of Pol II-mediated transcriptional elongation [14]. Either scenario would result in more time provided for the splicing machinery to recognize and include ASEs in the final transcript [13, 29] (Figure 7I). Indeed, our genome-wide data support this transcription-coupled model of alternative splicing regulation, as co-localization of elongating Ser2P-Pol II with MeCP2 occurred preferentially over included ASEs versus excluded ASEs. In addition, the distinct pattern of Ser2P-Pol II depletion at excluded ASEs relative to included ASEs and flanking constitutively spliced exons (Figure 5G) could arise from a higher Pol II elongation
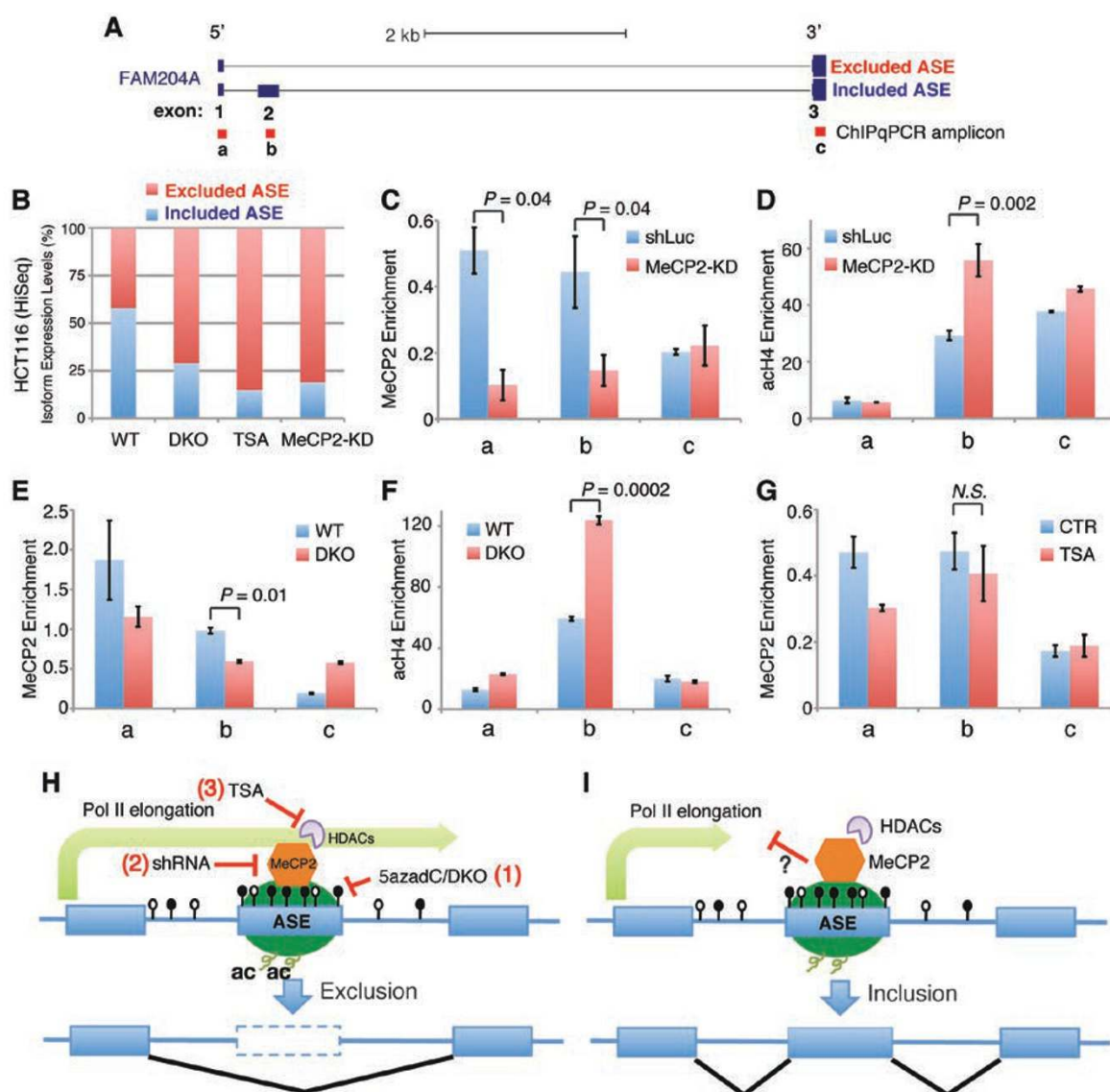
Figure 7 MeCP2 recruits HDAC activity, promoting local histone hypoacetylation and exon inclusion. **(A)** Schematic representation showing the partial structure of the *FAM204A* gene. The red squares (a, b, and c) below the gene indicate the locations of qPCR probes used for ChIP assays. **(B)** Comparison of expression level of *FAM204A* isoforms that excludes (red) or includes (blue) exon 2. Expression of the *FAM204A* isoforms was determined by RNA-Seq data analyzed by MISO (confirmed by qPCR, data not shown). The normalized expression levels are displayed as a percentage, where the total expression of the two isoforms sum to 100%. WT, HCT116-WT cells; DKO, HCT116-DKO cells; TSA, TSA-treated HCT116-WT cells; MeCP2-KD, MeCP2-knockdown HCT116-WT cells. **(C)** Knockdown of *MeCP2* decreased MeCP2 binding to the exon 1 (probe a) and ASE (probe b) regions of the *FAM204A* gene. MeCP2 occupancy at different DNA regions was measured using the ChIP assays with chromatin harvested from control (shLuc) or MeCP2-knockdown (MeCP2-KD) HCT116 cells, followed by quantification using the qPCR assays. **(D)** Knockdown of *MeCP2* resulted in a significant increase of histone acetylation over the ASE region (probe b). Acetylation level was measured using ChIP-qPCR assays with chromatin harvested from the cells as described in **C**. **(E)** DNA demethylation by DNMT-deficiency resulted in decreased binding of MeCP2 to the ASE region (probe b). MeCP2 binding was measured using ChIP-qPCR assays with chromatin harvested from HCT116-WT and HCT116-DKO cells. **(F)** DNA demethylation by DNMT-deficiency resulted in increased histone acetylation over the ASE region (probe b). MeCP2 binding was measured using ChIP-qPCR assays with chromatin harvested from HCT116-WT and HCT116-DKO cells. **(G)** Inhibition of HDAC activity did not significantly change the binding of MeCP2 to the ASE region. MeCP2 binding was measured using ChIP-qPCR assays with chromatin from untreated (CTR) and TSA-treated HCT116-WT cells. Error bars in **C-G** represent SE. *P*-values shown in **C-G** were calculated using one-sided Student's *t*-test. *N.S.*, not significant. **(H)** Cartoon showing the three independent treatments that downregulate the inclusion of ASEs: (1) inhibition of DNA methylation, (2) knockdown of *MeCP2* and (3) inhibition of HDAC activity using TSA treatment. **(I)** Model depicting the relationship of DNA methylation, MeCP2 binding, HDAC recruitment and Pol II elongation in exon recognition.

rate over excluded exons than that over included exons. Recently developed genome-wide assays aimed at measuring Pol II elongation rates, such as GRO-seq [30], can be used to more comprehensively explore the relationship between the kinetics of transcriptional elongation and alternative splicing.

We recognize that ASE regulation is complex, possibly involving multiple mechanisms depending on the target ASE and cell context. The aberrant ASE exclusion events we observed upon inhibiting DNA methylation or MeCP2 expression could also be explained by altered expression of splicing factors; however, our RNA-Seq data of DNMT- or MeCP2-deficient cells did not reveal significant changes in the expression levels of known splicing factors. This result supports our hypothesis that DNA methylation and MeCP2 binding are likely to influence pre-mRNA splicing patterns directly. In addition, nucleosome positioning has been suggested to play a role in pre-mRNA splicing [31]. The methods for genome-wide mapping of nucleosome positioning and DNA methylation level within individual DNA molecules [32] are likely to be essential for further defining the relationship between DNA methylation, nucleosome positioning and alternative pre-mRNA splicing [9].

Mutations in the gene encoding MeCP2 primarily account for the debilitating neurodevelopmental disorder Rett syndrome (RTT), an autism spectrum disorder [33, 34]. Mouse models of RTT exhibit RNA splicing defects [22]; however, whether these defects are relevant to human disease has yet to be investigated. Misregulation and sequence variants of *MeCP2* are found in patients with autism spectrum disorders [23, 35] and the autoimmune disorder systemic lupus erythematosus [36], respectively. Abnormal DNA methylation contributes to the etiology of these diseases [37-39]. Our study implicates the loss of function of DNA methylation and MeCP2 as a cause of altered pre-mRNA splicing, which could potentially contribute to disease development [40], a possibility that warrants further investigation.

Materials and Methods

Cells, antibodies and ChIP-Seq

Human IMR90 cells (American Type Culture Collection; ATCC) were cultured under optimal growth conditions as specified by ATCC, and only cells at early passage were used for experiments [15]. HCT116-WT and HCT116-DKO cells were generous gifts from Dr B Vogelstein (Johns Hopkins University) [17]. These cells were cultured in McCoy's 5A medium with 10% FBS. Chromatin from 5 million cells per ChIP was prepared by formaldehyde cross-linking and sonication as described previously [41]. Antibodies against MeCP2 (Abcam; ab2828), Ser2P-Pol II (Abcam; ab5095) or IgG (Upstate Biotechnology; 12-370) were added in manufacturer-recommended amounts per ChIP. A home-made pan-acetylH4 antibody [42] was used for acetylation ChIP. For input control samples, DNA was isolated from 10% (vol.) of chromatin material used for ChIP by phenol/chloroform extraction and ethanol purification procedures [41]. ChIP-Seq was carried out using the remaining chromatin according to established protocols [41] and prepared libraries were sequenced with the Illumina Genome Analyzer II sequencer according to the manufacturer's instructions.

ChIP-qPCR

Immunoprecipitated DNA and input DNA were analyzed by SYBR-Green real-time quantitative PCR. PCR was performed using primers targeting exon 10 of *HAUS8* and selected areas over the "cassette" exon regions of *FAM204A* with the SYBR Green PCR master mix (Applied Biosystems; ABI) and measured in a 7900HT fast real-time PCR system (ABI) according to the manufacturer's protocol. PCR measurements were performed in triplicate for each sample and enrichment was calculated as a percentage relative to input controls using the delta-C_t method. Primer sequences are listed in Supplementary information, Table S1.

Target sequence of shMeCP2, virus production and infection

MeCP2 shRNA, 5′-CATTAGGGTCCAGGGATGTGT-3′; shRNA constructs were designed and cloned into the pGreenPuro lentiviral vector according to the specifications provided by System Biosciences and their shLuc construct was used as a negative, nonspecific control. Sequences were confirmed by automated DNA sequencing (not shown). The shMeCP2 and shLuc constructs were transfected into HEK-293T cells for packaging according to System Biosciences' instructions. Viral supernatants were collected for infection of IMR90 cells. 2×10^6 early passage IMR90 cells or HCT116-WT cells were seeded in the presence of viral supernatant and 8 μg/ml polybrene per well of a 12-well plate. After 24 h, cells were trypsinized and transferred into 6-well plates with fresh media and 5 μg/ml puromycin. Selection was visually monitored by GFP positivity and cells were collected for experiments at day 3 post-infection when > 95% of cells by count were GFP positive.

Demethylation and deacetylation experiments

Primary IMR90 cells were seeded at 1×10^5 cells per well of a 6-well plate, incubated for 24 h in Eagle's Minimum Essential Medium (EMEM, ATCC) high glucose with 10% serum, and then supplemented with fresh media containing 20 μM 5azadC (Sigma-Aldrich) for 72 h. Media containing drug was changed every 24 h. For HDAC inhibition, IMR90 or HCT116-WT cells were seeded at a density of 2×10^6 cells in 100-mm plates with EMEM or McCoy's 5A medium (ATCC) supplemented with 10% serum, respectively, incubated overnight, and mock treated (media only; "CTR") or treated with 300 nM TSA (Sigma-Aldrich) for 6 h in an CO_2 incubator at 37 °C.

DNA isolation

Cells were lysed in DNA extraction buffer (50 mM Tris pH 8.0, 0.5% sodium dodecyl sulfate, 0.5 mM EDTA pH 8.0, and 1 mg/ml proteinase K) overnight at 65 °C. RNA was removed with RNase treatment (40 μg/ml, Roche DNase-free RNase) for 1 h at 37 °C. DNA was purified by PCI (25:24:1) extractions followed by pre-

cipitation with sodium acetate and ethanol. The DNA pellet was resuspended in TE buffer.

Bisulfite treatment, PCR and sequencing

Total genomic DNA was treated with sodium bisulfite (Sigma-Aldrich) for 16 h as previously reported [7]. The *HAUS8* locus was amplified by PCR using primers listed in Supplementary information, Table S1, and amplicons were cloned into pCR2.1/TOPO (Invitrogen). We selected a specified number of individual transformed colonies and sequenced inserts using the ABI 3700 automated DNA sequencer. DNA methylation patterns and levels were determined only from highly (> 95%) converted sequences.

RNA extraction and RNA-Seq

Total mRNA was isolated from all cells using the RNeasy kit (Qiagen) and converted to cDNA using the Superscript ds-cDNA synthesis kit (Invitrogen) according to the manufacturer's instructions. For RNA-Seq, double-stranded DNAs were fragmented to 100–200 bp using sonication, followed by end-repair, Illumina adaptor ligation and sequencing using the Illumina HiSeq 2000 platform according to the manufacturer's protocol for paired-end reads.

Quantitative RT-PCR

Double-stranded cDNA synthesized from RNA isolated with the RNeasy Mini Kit (Qiagen) using SuperScript II (Introgen) according to the manufacturer's instructions. For *FAM204A* expression, quantitative RT-PCR was carried out using primers specific to each isoform to target expression of those that included or excluded exon 2 with the SYBR Green PCR master mix (Applied Biosystems) in a 7900HT fast real-time PCR system (ABI) according to the manufacturer's protocol. Primers and PCR conditions used for amplification are listed in Supplementary information, Table S1. PCRs were performed in triplicate from each sample and expression was calculated as a percentage relative to *ACTB* using the delta-C_t method.

Western blots

Cells were lysed in the SDS protein gel-loading solution (Quality Biological Inc.). Equal amounts of protein (20 µg) were loaded per lane on a 4% - 20% gradients SDS-PAGE gel and transferred onto nitrocellulose membranes (Schleicher & Schuell Bioscience; Protran). Western blot was performed with anti-MeCP2 (Abcam; ab2828) or anti-β-actin (Abcam; ab6276) antibodies according to the manufacturer's recommendations. Detection was carried out using the ECL Plus Western Blotting Detection System (GE Healthcare) exposed on Biomax MR film (Kodak).

Data analysis and statistics

Quality-filtered Illumina sequencing reads from ChIP-Seq libraries were aligned to hg18 human genome using Bowtie software. The sequencing reads from RNA-Seq libraries were mapped to hg18 genome using TopHat algorithm (version 1.3.1) [43]. To avoid possible PCR artifacts, no more than one uniquely aligned read per strand was kept. Where applicable, publically available data were used in our analyses and cited in the text.

For the libraries that involved sonication procedure, the average ChIP fragment lengths were estimated using strand cross-correlation profiles as previously described [44] and the forward and reverse strand tag locations were shifted accordingly. For the IMR90 nucleosome library, tags were shifted by 75 bp.

UCSC genome browser displayable bedGraph files for ChIP-Seq data were generated by counting shifted tags in 200-bp windows across the genome and normalizing window tag counts by 5 million total sequenced reads to make different libraries directly comparable. We controlled for any potential enrichment due to nonspecific antibody selection or PCR bias using ChIP-Seq libraries of IgG preimmune sera as described previously [41]. Thus, library-size-normalized shifted IgG ChIP-Seq tag counts were subtracted to control for any potential "background" enrichment. Normalized and background subtracted bedGraph files generated as described were used for all UCSC browser figures. For RNA-Seq data, tags were not shifted and 20-bp windows were used. The number of tags in each 20-bp window was normalized to represent local RPKM value in the window.

Genomic binding sites were identified from ChIP-Seq data using local Poisson background models estimated from IgG control data as described previously [45]. False discovery rate cutoff of 10% was used to retain significant sites.

To determine the genomic distribution of MeCP2 sites, we defined promoters as regions 2-kb upstream of Ensembl annotated transcription start sites and excluded parts of the regions that overlapped gene bodies. Intergenic regions were defined as non-genic and non-promoter regions. Intronic regions were defined as introns that do not overlap exons from any annotated transcript.

Average MeCP2 density profiles at splice acceptor sites of constitutive exons in Figure 3B were generated by counting tags in 30-bp intervals in 600-bp windows centered at the acceptor sites and re-scaling the counts to represent densities per 100 bp.

To generate the DNA methylation, MeCP2 and Ser2P-Pol II density profiles at ASE exons, displayed in Figures 1B, 4 and 5G, we extracted the database of "cassette" exons that is included in the MISO software package (version 0.2). The inclusion levels (Ψ) of ASE exons were estimated using the MISO algorithm with the following default parameters: filter_results = True and min_event_reads = 20. The exons with inclusion level $\Psi \geq 0.9$ were regarded as "included exons" and those with $\Psi \leq 0.1$ were regarded as "excluded exons". Only ASEs whose 5′ exons were more than 2-kb away from annotated transcription start sites are represented to avoid potentially confounding signal from promoter-bound MeCP2. The CpG-density normalized DNA methylation level for each small genomic interval in Figure 1B was defined as the sum of DNA methylation levels of all CpGs in the interval divided by the total number of CpGs in the interval.

The *P*-values for the relative enrichment of MeCP2 (Figure 4), Ser2P-Pol II (Figure 5G) and CpG methylation (Figure 1B) in included compared to excluded exons were calculated using one-sided *t*-test for sequence read density (MeCP2 and Ser2P-Pol II) or the normalized DNA methylation in the exons.

The *P*-value for the depletion of Ser2P-Pol II at excluded ASE relative to flanking constitutive exons was calculated as follows: For each ASE, we computed the enrichment of Ser2P-Pol II at ASE as the ratio λ of Ser2P-Pol II read density at ASE to the density at flanking constitutive exons. The mean values of λ in "included ASE" and "excluded ASE" groups were then compared and the one-sided *t*-test was used to compute *P*-value.

Statistical testing for co-localization of MeCP2 and CpG methylation in constitutive exons (Figure 3C) was performed us-

ing two-ranked lists of constitutive exons as follows: List A was ranked by MeCP2 density in descending order. List B was ranked by CpG methylation density in descending order. Thus, A[1] is the constitutive exon with highest MeCP2 density and B[1] is the constitutive exon with the highest CpG methylation density. The top n MeCP2- and CpG methylation-dense constitutive exons lists are A[1:n] and B[1:n], respectively. Let k be the number of exons shared between the two top n lists. If k is significantly larger than the number expected by chance, MeCP2 and CpG methylation co-localize in exons. If k is significantly less than the number expected by chance, MeCP2 and CpG methylation are mutually exclusive in exons. The P-value for each n is computed based on binomial distribution and are the medians of P-values for all possible values of n shown on the x-axis.

The differential ASE up-/downregulation between control and test samples (Figures 2A, 5C and 6A) was determined as follows: The exons with the inclusion level change $\Delta\Psi > 0.1$ were regarded "aberrantly downregulated" and those with $\Delta\Psi < -0.1$ were regarded as "aberrantly upregulated". The Bayes factors determined by MISO for differentially up-/downregulated exons were required to be greater than 2. The MISO analysis was performed on parallel computing clusters at the NIH Biowulf supercomputing facility. For Figure 5D-5F, the MeCP2 or nucleosome tag density at differentially upregulated and downregulated exons in control cells were computed and one-sided Wilcoxon rank-sum test was used to determine statistical significance.

Relative isoform expression levels reported in Figure 7B were calculated from inclusion levels of exon 2 of *FAM204A* gene estimated using MISO as described above. The P-values for Figure 6A were calculated using one-sided binomial test assuming that ASE up- and downregulation events are equally likely (null hypothesis). The P-value for each comparison in Figure 6D was calculated using χ^2-test for the 2×2 table of the numbers of up/downregulated ASEs upon MeCP2-KD that are also up/downregulated upon TSA (2 numbers) and the numbers of up/downregulated ASEs upon MeCP2-KD that are also not-up/not-downregulated upon TSA (2 numbers).

The GEO accession number for the raw and processed data described in this article is GSE47678.

Acknowledgments

References

1   Chen ZX, Riggs AD. DNA methylation and demethylation in mammals. *J Biol Chem* 2011; **286**:18347-18353.

2   Jones PA, Takai D. The role of DNA methylation in mammalian epigenetics. *Science* 2001; **293**:1068-1070.

3   Klose RJ, Bird AP. Genomic DNA methylation: the mark and its mediators. *Trends Biochem Sci* 2006; **31**:89-97.

4   Deaton AM, Webb S, Kerr AR, *et al.* Cell type-specific DNA methylation at intragenic CpG islands in the immune system. *Genome Res* 2011; **21**:1074-1086.

5   Illingworth R, Kerr A, Desousa D, *et al.* A novel CpG island set identifies tissue-specific methylation at developmental gene loci. *PLoS Biol* 2008; **6**:e22.

6   Liang P, Song F, Ghosh S, *et al.* Genome-wide survey reveals dynamic widespread tissue-specific changes in DNA methylation during development. *BMC Genomics* 2011; **12**:231.

7   Maunakea AK, Nagarajan RP, Bilenky M, *et al.* Conserved role of intragenic DNA methylation in regulating alternative promoters. *Nature* 2010; **466**:253-257.

8   Anastasiadou C, Malousi A, Maglaveras N, Kouidou S. Human epigenome data reveal increased CpG methylation in alternatively spliced sites and putative exonic splicing enhancers. *DNA Cell Biol* 2011; **30**:267-275.

9   Chodavarapu RK, Feng S, Bernatavichute YV, *et al.* Relationship between nucleosome positioning and DNA methylation. *Nature* 2010; **466**:388-392.

10   Choi JK. Contrasting chromatin organization of CpG islands and exons in the human genome. *Genome Biol* 2010; **11**:R70.

11   Feng S, Cokus SJ, Zhang X, *et al.* Conservation and divergence of methylation patterning in plants and animals. *Proc Natl Acad Sci USA* 2010; **107**:8689-8694.

12   Shukla S, Kavak E, Gregory M, *et al.* CTCF-promoted RNA polymerase II pausing links DNA methylation to splicing. *Nature* 2011; **479**:74-79.

13   Luco RF, Allo M, Schor IE, Kornblihtt AR, Misteli T. Epigenetics in alternative pre-mRNA splicing. *Cell* 2011; **144**:16-26.

14   Lorincz MC, Dickerson DR, Schmitt M, Groudine M. Intragenic DNA methylation alters chromatin structure and elongation efficiency in mammalian cells. *Nat Struct Mol Biol* 2004; **11**:1068-1075.

15   Lister R, Pelizzola M, Dowen RH, *et al.* Human DNA methylomes at base resolution show widespread epigenomic differences. *Nature* 2009; **462**:315-322.

16   Mossman D, Kim KT, Scott RJ. Demethylation by 5-aza-2′-deoxycytidine in colorectal cancer cells targets genomic DNA whilst promoter CpG island methylation persists. *BMC Cancer* 2010; **10**:366.

17   Rhee I, Bachman KE, Park BH, *et al.* DNMT1 and DNMT3b cooperate to silence genes in human cancer cells. *Nature* 2002; **416**:552-556.

18   Wozniak RJ, Klimecki WT, Lau SS, Feinstein Y, Futscher BW. 5-Aza-2′-deoxycytidine-mediated reductions in G9A histone methyltransferase and histone H3 K9 di-methylation levels are linked to tumor suppressor gene reactivation. *Oncogene* 2007; **26**:77-90.

19   Schor IE, Rascovan N, Pelisch F, Allo M, Kornblihtt AR. Neuronal cell depolarization induces intragenic chromatin modifications affecting NCAM alternative splicing. *Proc Natl Acad Sci USA* 2009; **106**:4325-4330.

20   Nan X, Meehan RR, Bird A. Dissection of the methyl-CpG binding domain from the chromosomal protein MeCP2. *Nucle-*

ic Acids Res 1993; **21**:4886-4892.

21 Long SW, Ooi JY, Yau PM, Jones PL. A brain-derived MeCP2 complex supports a role for MeCP2 in RNA processing. *Biosci Rep* 2011; **31**:333-343.

22 Young JI, Hong EP, Castle JC, *et al.* Regulation of RNA splicing by the methylation-dependent transcriptional repressor methyl-CpG binding protein 2. *Proc Natl Acad Sci USA* 2005; **102**:17551-17558.

23 Yasui DH, Peddada S, Bieda MC, *et al.* Integrated epigenomic analyses of neuronal MeCP2 reveal a role for long-range interaction with active genes. *Proc Natl Acad Sci USA* 2007; **104**:19416-19421.

24 Nan X, Ng HH, Johnson CA, *et al.* Transcriptional repression by the methyl-CpG-binding protein MeCP2 involves a histone deacetylase complex. *Nature* 1998; **393**:386-389.

25 Ip JY, Schmidt D, Pan Q, *et al.* Global impact of RNA polymerase II elongation inhibition on alternative splicing regulation. *Genome Res* 2011; **21**:390-401.

26 Allo M, Schor IE, Munoz MJ, *et al.* Chromatin and alternative splicing. *Cold Spring Harb Symp Quant Biol* 2010; **75**:103-111.

27 Zhou HL, Hinman MN, Barron VA, *et al.* Hu proteins regulate alternative splicing by inducing localized histone hyperacetylation in an RNA-dependent manner. *Proc Natl Acad Sci USA* 2011; **108**:E627-635.

28 Wood AJ, Schulz R, Woodfine K, *et al.* Regulation of alternative polyadenylation by genomic imprinting. *Genes Dev* 2008; **22**:1141-1146.

29 de la Mata M, Alonso CR, Kadener S, *et al.* A slow RNA polymerase II affects alternative splicing *in vivo. Mol Cell* 2003; **12**:525-532.

30 Core LJ, Waterfall JJ, Lis JT. Nascent RNA sequencing reveals widespread pausing and divergent initiation at human promoters. *Science* 2008; **322**:1845-1848.

31 Tilgner H, Nikolaou C, Althammer S, *et al.* Nucleosome positioning as a determinant of exon recognition. *Nat Struct Mol Biol* 2009; **16**:996-1001.

32 Kelly TK, Liu Y, Lay FD, Liang G, Berman BP, Jones PA. Genome-wide mapping of nucleosome positioning and DNA methylation within individual DNA molecules. *Genome Res* 2012; **22**:2497-2506.

33 Amir RE, Van den Veyver IB, Wan M, Tran CQ, Francke U, Zoghbi HY. Rett syndrome is caused by mutations in X-linked MECP2, encoding methyl-CpG-binding protein 2. *Nat Genet* 1999; **23**:185-188.

34 LaSalle JM, Hogart A, Thatcher KN. Rett syndrome: a Rosetta stone for understanding the molecular pathogenesis of autism. *Int Rev Neurobiol* 2005; **71**:131-165.

35 Moretti P, Zoghbi HY. MeCP2 dysfunction in Rett syndrome and related disorders. *Curr Opin Genet Dev* 2006; **16**:276-281.

36 Webb R, Wren JD, Jeffries M, *et al.* Variants within MECP2, a key transcription regulator, are associated with increased susceptibility to lupus and differential gene expression in patients with systemic lupus erythematosus. *Arthritis Rheum* 2009; **60**:1076-1084.

37 Nagarajan RP, Hogart AR, Gwye Y, Martin MR, LaSalle JM. Reduced MeCP2 expression is frequent in autism frontal cortex and correlates with aberrant MECP2 promoter methylation. *Epigenetics* 2006; **1**:e1-e11.

38 Nagarajan RP, Patzel KA, Martin M, *et al.* MECP2 promoter methylation and X chromosome inactivation in autism. *Autism Res* 2008; **1**:169-178.

39 Lei W, Luo Y, Lei W, *et al.* Abnormal DNA methylation in CD4+ T cells from patients with systemic lupus erythematosus, systemic sclerosis, and dermatomyositis. *Scand J Rheumatol* 2009; **38**:369-374.

40 Tazi J, Bakkour N, Stamm S. Alternative splicing and disease. *Biochim Biophys Acta* 2009; **1792**:14-26.

41 Barski A, Cuddapah S, Cui K, *et al.* High-resolution profiling of histone methylations in the human genome. *Cell* 2007; **129**:823-837.

42 Wan M, Zhao K, Lee SS, Francke U. MECP2 truncating mutations cause histone H4 hyperacetylation in Rett syndrome. *Hum Mol Genet* 2001; **10**:1085-1092.

43 Trapnell C, Pachter L, Salzberg SL. TopHat: discovering splice junctions with RNA-Seq. *Bioinformatics* 2009; **25**:1105-1111.

44 Kharchenko PV, Tolstorukov MY, Park PJ. Design and analysis of ChIP-seq experiments for DNA-binding proteins. *Nat Biotechnol* 2008; **26**:1351-1359.

45 Zhang Y, Liu T, Meyer CA, *et al.* Model-based analysis of ChIP-Seq (MACS). *Genome Biol* 2008; **9**:R137.

46 Hahn MA, Wu X, Li AX, Hahn T, Pfeifer GP. Relationship between gene body DNA methylation and intragenic H3K9me3 and H3K36me3 chromatin marks. *PLoS One* 2011; **6**:e18844.

(**Supplementary information** is linked to the online version of the paper on the *Cell Research* website.)